



# Structure and strength of Al-Mn-Cu-Zr-Cr-Fe ALTEC alloy after radial-shear rolling

A. N. Petrova<sup>†,1</sup>, D. Yu. Rasposienko<sup>1</sup>, V. V. Astafyev<sup>1</sup>, A. O. Yakovleva<sup>2</sup>

<sup>†</sup>petrovanastya@yahoo.com

<sup>1</sup>M. N. Mikheev Institute of Metal Physics of UB of RAS, Ekaterinburg, 620108, Russia

<sup>2</sup>National university of science and technology MISIS, Moscow, 119049, Russia

The phase composition and structure of as-cast and deformed Al-1.53Cu-1.66Mn-0.38Zr-0.15Cr-0.15Fe (wt.%) were investigated. The radial shear rolling was used for the deformation of the alloy. The structure of as-cast alloy consists of aluminum solid solution, eutectic Al<sub>6</sub>(FeMn) and Al<sub>2</sub>Cu, as well as Al<sub>7</sub>Cr and Al<sub>20</sub>Cu<sub>2</sub>Mn<sub>3</sub> dispersive particles. It is assumed that radial shear rolling results in the refinement and partial dissolution of Al<sub>20</sub>Cu<sub>2</sub>Mn<sub>3</sub> dispersoids. Along with this, significant grain refinement was established after deformation. The average grain-subgrain size in the alloy after deformation is 1.6 μm. After deformation the alloy has the yield stress of 83 MPa and ultimate strength of 216 MPa. The elongation to failure of the deformed alloy is 25%. Owing to the partial deformation induced dissolution of the aluminides and supersaturated solid solution formation, there is a potential for strengthening upon heat treatment of the alloy and improvement of its thermal resistance.

**Keywords:** Al-Cu-Mn-Zr system, severe plastic deformation, radial shear rolling, strength, plasticity, phase composition.

## 1. Introduction

Developing materials with predetermined properties at present remains relevant in the scientific community. This is often a goal of increasing the mechanical strength of materials, while maintaining sufficient ductility and increasing heat resistance. This is especially true for aluminum alloys, whose strength properties at room and elevated temperatures impose certain restrictions on their use. It is necessary to use efficient methods of deformation and heat treatment to improve the structure and performance properties of aluminum alloys. It is known that one of the methods for increasing the strength is to reduce the grain size of an aluminium matrix. Using severe plastic deformation (SPD) methods allows one, in addition to the grain refinement, to obtain a supersaturated aluminum solid solution (for further aging during the heat treatment of the alloy), disperse the second phases, initiate dynamic ageing and change phase transformation kinetics [1–3]. These methods, unlike industrial deformation techniques such as rolling, pressing, drawing, allow one to impart large plastic deformations (accumulated deformation  $e > 1$ ) to the material. For example, high pressure torsion in Bridgman's anvils is a laboratory method that allows the deformation of a material to very large strains (depending on the angle of the anvil rotation) without changing its geometric sizes. The disadvantage of this method is that the size of the samples produced is limited. In turn, radial shear rolling (RSR) is an industrial method that allows fabricating large-scale semi-finished products and accumulating strains up to  $e = 4$ .

Ultrafine-grained materials with a grain size of less than 1 μm have shown increased strength, plasticity and a

number of other properties attractive for a variety of practical applications. In particular, it has been shown that dispersion-hardened Al alloys of the Al-Zn-Mg-Cu system after SPD have strength of 750–1000 MPa, which is significantly higher than the strength of coarse-grained alloys [4]. The studies have proved that the strength of aluminum alloys depends not only on the grain size, but an important factor influencing the strengthening is the local chemical composition of the grain boundaries of ultrafine-grained and nanostructured materials [5–9]. In particular, in highly-deformed alloys there may be a segregation of atoms and clusters at grain boundaries due to different diffusion coefficients of alloying elements and the matrix. These results gave impetus to the development of studies aimed at improving the properties of Al alloys by controlling the state of their grain boundaries.

On an example of Al-Mn-Cu (Zr, Cr) ALTEC alloys [10–13], it is shown that when copper is added in a quantity of less than 2 wt.%, most of it dissolves in aluminium. This makes it possible to deform the ingots without the homogenization, which is an essential technological step for most industrial aluminium alloys [13]. ALTEC alloys differ significantly from their 2xxx system analogues (for example, the widely used industrial alloy AA2219). In particular, after annealing the alloy contains nano-sized Al<sub>3</sub>Zr particles and dispersed Al<sub>20</sub>Cu<sub>2</sub>Mn<sub>3</sub> phase particles with a size of 500 nm [10]. This structure ensures high strength properties and good heat resistance.

The aim of this work is to reveal the potential for improving the physical and mechanical properties of the Al-Cu-Mn model ALTEC alloy using severe plastic deformation method by means of radial shear rolling.

## 2. Materials and experimental techniques

The phase composition of a model Al-1.8Mn-1.6Cu-0.4Zr-0.15Cr-0.15Fe (wt.%) alloy was calculated using the Thermo-Calc (TCW5) program [14]. The TTAL5 data base was used for calculations. At these alloying element concentrations, polythermal section of the Al-Mn-Cu-Zr-Cr-Fe system was obtained. The temperature dependence of the mass fractions of solid phases was calculated for Al-1.8Mn-1.6Cu-0.4Zr-0.15Cr-0.15Fe alloy according to Sheil-Goulliver model [15,16].

The alloy was prepared in an electric resistance furnace in a graphite-shamote crucible. Primary aluminium A85, copper grade M1, Al-10%Mn, Al-10%Zr and Al-10%Cr master alloys were used as charging materials. The melt was poured at 900°C to a graphite mold with a diameter of 40 mm. The actual chemical composition of the experimental alloy was Al-1.53Cu-1.66Mn-0.38Zr-0.15Cr-0.15Fe (wt.%).

The ingots were deformed by the radial-shear rolling (RSR) method at a temperature of 280°C. RSR was carried out in two passes according to the scheme  $\varnothing 40 \rightarrow \varnothing 31 \rightarrow \varnothing 24$  mm without intermediate annealing on an experimental-industrial mill. The total drawing ratio was  $\mu = 3.4$ .

The structure of the materials was investigated using a Quanta 200 scanning electron microscope equipped with EDAX energy dispersive spectrometer (EDS) and a Tescan Mira scanning electron microscope equipped with Oxford Instruments UltimXmax energy dispersive spectrometer and Oxford Instruments CMOS EBSD Symmetry electron backscatter diffraction detector. The samples for structural analysis were prepared by mechanical grinding and subsequent polishing with a diamond suspension. The final polishing was carried out using a suspension of colloidal silicon dioxide.

The macrostructure investigation was carried out by means of optical microscopy. Sample preparation included mechanical grinding and polishing, etching in Keller solution (0.5 ml HF, 2.5 ml HNO<sub>3</sub>, 1.5 ml HCl, 100 ml H<sub>2</sub>O).

X-ray analysis was carried out on a laboratory Bruker Advance-D8 diffractometer in the CuK<sub>α</sub>-radiation ( $K_{\alpha,av} = 0.15418$  nm) in the range of 18–140° with a step of 0.02° and exposure time of 2 s. The processing of the diffraction

patterns received was carried out using the DIFFRAC. EVA 4.0 and DIFFRAC. TOPAS 5.0 software and PDF 2.1202 data base.

Static mechanical tests were carried out using Instron 5982 universal testing machine. Bone shaped flat samples with the gauge length of 27 mm, width of 7 mm and thickness of 4 mm were used. The tensile tests were conducted at room temperature and at strain rate of  $\dot{\epsilon} = 1.5 \times 10^{-3} \text{ s}^{-1}$ . At least 3 specimens were tested for each state of the alloy.

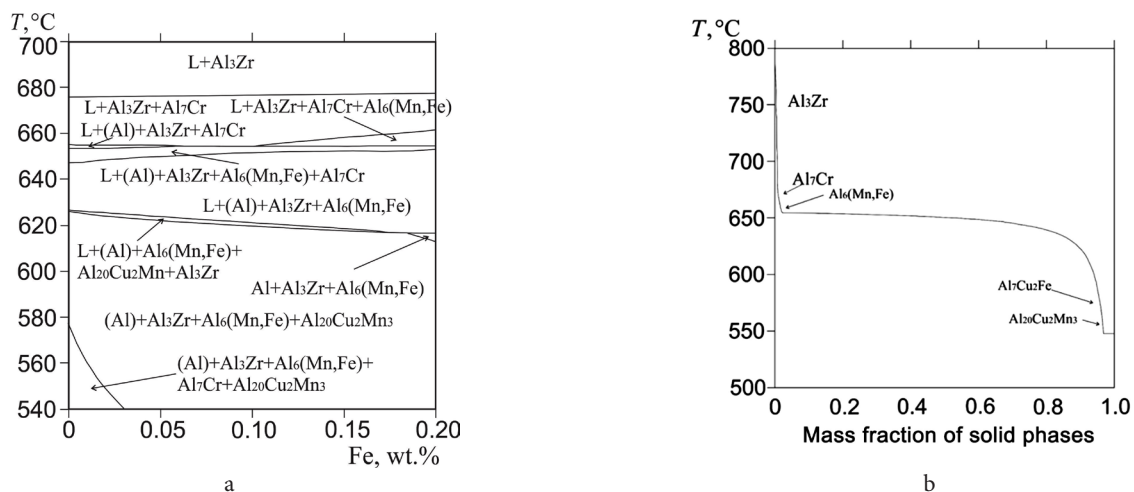
## 3. Experimental results

Figure 1a shows a polythermal section of the Al-Mn-Cu-Zr-Cr-Fe system calculated at constant concentrations of copper, manganese, zirconium and chromium: 1.8%Mn, 1.6%Cu, 0.4%Zr and 0.15%Cr (wt.%). The alloy liquidus is about 800°C, which is due to the high concentration of zirconium. The solidus is to be around 630°C. Since iron is inevitably present even in the best grades of technical aluminium, the calculations have shown that even at low concentrations of iron the phases Al<sub>6</sub>(Fe, Mn) and Al<sub>7</sub>Cu<sub>2</sub>Fe can be formed.

Since the cast structure is formed under nonequilibrium crystallization conditions, the dependence of the mass fraction of solid phases on temperature was calculated for Al-1.8Mn-1.6Cu-0.4Zr-0.15Cr-0.15Fe alloy using Sheil-Goulliver model (Fig. 1b). From the dependencies obtained it follows that in non-equilibrium conditions the solidus is about 550°C, which is due to the formation of the Al<sub>2</sub>Cu phase as a part of the eutectic. According to the calculation results in the Al-1.8Mn-1.6Cu-0.4Zr-0.15Cr-0.15Fe alloy, in addition to the aluminum solid solution, Al<sub>20</sub>Cu<sub>2</sub>Mn<sub>3</sub>, Al<sub>2</sub>Cu, Al<sub>6</sub>(Fe, Mn), Al<sub>3</sub>Zr D023, Al<sub>7</sub>Cr, Al<sub>7</sub>Cu<sub>2</sub>Fe phases may be present after crystallization.

Figure 2 shows the cast structure of the alloy. Two zones can be distinguished on the macrosection. One is the central region of equiaxial grains which are about 2 mm in size. The other is the area of directional solidification with much larger grains of 4–6 mm in size.

By means of scanning electron microscope, the crystallization phases were established in the alloy structure (Fig. 3). Figure 3a shows elongated eutectic globular particles. Eutectic filling consists of two types of particles.



**Fig. 1.** The results of phase composition calculations for the Al-Mn-Cu-Zr-Cr-Fe system: polythermal section at concentration of alloying elements of 1.8%Mn, 1.6%Cu, 0.4%Zr, 0.15 Cr (a), dependence of the mass fraction of solid phases on the temperature for Al-1.8Mn-1.6Cu-0.4Zr-0.15Cr-0.15Fe alloy (b).

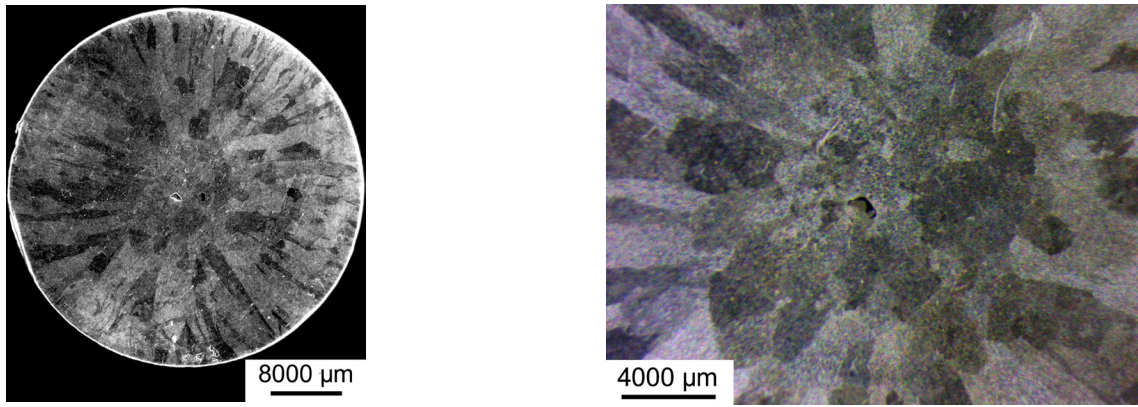


Fig. 2. Macrostructure in as-cast alloy.

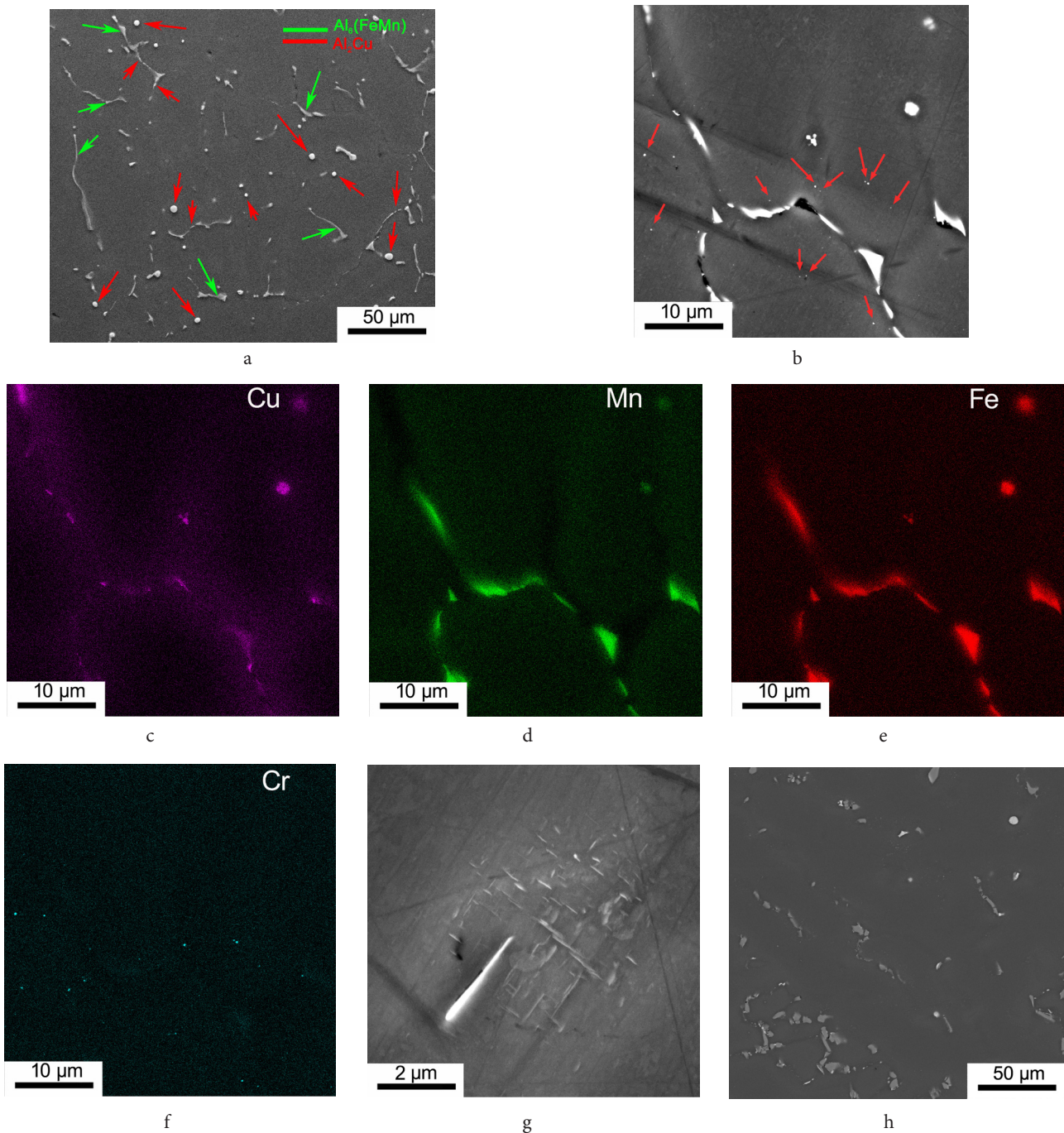


Fig. 3. (Color online) Structure of the alloy (SEM): as-cast alloy (a) – (g), deformed alloy (h), back scattered electron image (a), (b), (g), (h), eutectic  $Al_2Cu$  and  $Al_6(Fe, Mn)$  (a), (b), EDS mapping (c) – (f),  $Al_{20}Cu_2Mn_3$  (g).

Elemental analysis showed that one phase was enriched with manganese, iron, and copper (phase  $Al_6(Fe, Mn)$ ) (Fig. 3b–e). It is known that these alluminides contain Mn and Fe in a range of concentration and up to 0.2% Cu can be dissolved in  $Al_6(Fe, Mn)$  [17]. The globular phase is enriched with copper and lacks manganese as in the small particles in the eutectic filling. This is  $Al_2Cu$  phase. The element mapping also revealed a chromium phase and a copper-manganese phase. The  $Al_7Cr$  phase is marked by arrows on Fig. 3b. EDS analysis revealed that the particles shown in Fig. 3g were enriched with Cu and Mn, compared with the matrix. The results of EDS analysis are presented in Table 1. This is supposed to be  $Al_{20}Cu_2Mn_3$  phase.

Qualitative X-ray phase analysis confirms the data obtained with SEM. Thus, the large intensity peaks of (110), (220), (112)  $Al_2Cu$ , (110), (113)  $Al_6(Fe, Mn)$ , (113), (102-2), (51-5)  $Al_7Cr$  and (151), (200), (332), (333), (400)  $Al_{20}Cu_2Mn_3$  are validly determined on the diffraction pattern of as-cast alloy (Fig. 4).

RSR did not change the phase composition. All phases detected in the as-cast alloy are found in the deformed one. However, the shape of the  $Al_6(Fe, Mn)$  crystals changes. Brittle elongated crystals are fractured and become predominantly equiaxed (Fig. 3h). The average particle size increases from 18  $\mu m$  for the cast state to 6  $\mu m$  after the RSR. The size of the  $Al_2Cu$  crystallization phase does not change and is 3  $\mu m$  in average (Fig. 3h). According to comparison of the as-cast and deformed alloy diffraction patterns, the refinement of  $Al_{20}Cu_2Mn_3$  phase particles and their partial dissolution

occur during RSR. The peaks with relatively high intensity of (151), (200), (333), (400) reflexes of the  $Al_{20}Cu_2Mn_3$  phase are absent on the diffraction pattern after deformation (Fig. 4).

The RSR leads to a significant grain refinement in aluminum matrix. The band structure with mainly equiaxial substructure fragments (Fig. 5a) is formed. The fraction of grains with a misorientation angle of more than 15° is 33%. The subgrains with a misorientation angle more than 2° and less than 15° is 67% (Fig. 5b). According to EBSD data, the average grain-subgrain size is 1.6  $\mu m$ .

The mechanical tensile properties are presented in Table 2. After RSR, the yield stress of the alloy increases by 45%, the ultimate strength increases by 30%, while the material maintains good ductility.

#### 4. Discussion

In [18], high pure aluminium (Al 99.99%) and copper (Cu 99.9%) were used for melting a model aluminium-copper-manganese alloy. The authors reduced the iron content of the model alloy to 0.02 wt.%. The cast alloy structure consisted of two phases, Al solid solution and eutectic  $Al_2Cu$ , and all manganese was distributed in the solid solution. The volume fraction of  $Al_2Cu$  phase was negligible. Thus, most of the copper was also in the Al solid solution. After cold rolling and annealing at 300–400°C, dispersoids of high volume fraction were found in the alloy microstructure. Changing of the phase composition of the Al-1.97Cu-1.75Mn alloy during annealing includes decomposition of the Al solid solution with  $Al_{20}Cu_2Mn_3$  precipitation and dissolution of the eutectic  $Al_2Cu$  phase. At the same time, for the Al-5.86Cu-0.32Mn (AA 2219) alloy  $Al_{20}Cu_2Mn_3$  particles formed during homogenization

**Table 1.** EDS by point analysis results.

Point	Mn, wt.%	Cu, wt.%
1	1.64	4.48
2	1.12	5.25
3	1.62	4.28
4	1.58	4.76
5	0.33	2.28
6	0.40	1.86

**Table 2.** Mechanical properties of the alloy.

Material	YS <sub>0.2</sub> , MPa	UTS, MPa	$\delta$ , %
As-cast	57	166	22
After RSR	83	216	25

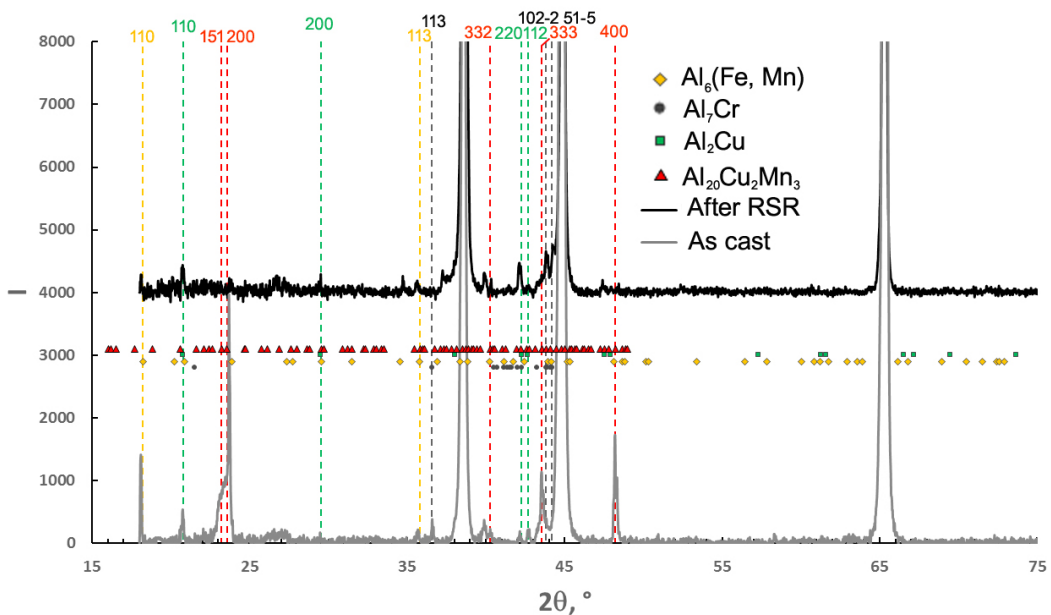


**Fig. 4.** (Color online) X-ray diffraction patterns of as-cast and RSR alloy.

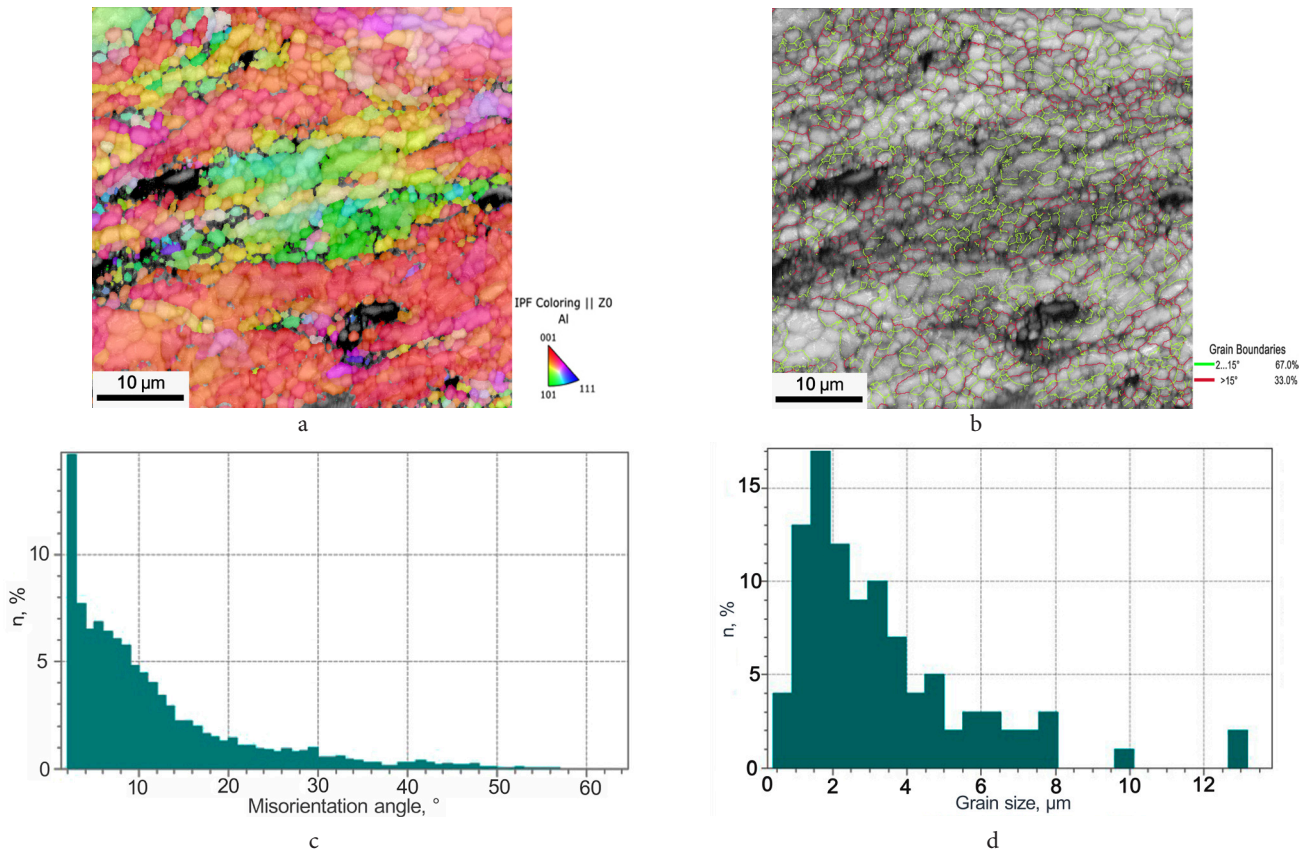


**Fig. 5.** (Color online) The RSR alloy structural characterization results obtained by means of EBSD: orientation map (a), misorientation angles distribution (b), grain-subgrain size distribution (c).

have been shown to remain unchanged during the whole processing route including cold rolling, artificial aging and annealing [18]. In commercial Al-Cu alloys,  $\text{Al}_3\text{Zr}$  particles are formed during homogenization at high temperature of about  $530^\circ\text{C}$ . They have comparatively large sizes [19].

In [10], Al-1.74Cu-1.57Mn-0.25Zr-0.11Sc-0.24Fe alloy was investigated. The authors did not report the formation of the  $\text{Al}_6(\text{Fe},\text{Mn})$  phase in the alloy. The formation of  $\text{Al}_{20}\text{Cu}_2\text{Mn}_3$  and nanosized  $\text{Al}_3(\text{Zr},\text{Sc})$  precipitates after rolling and annealing was established. According to phase composition calculations at 1.5% Cu, the increase in concentration of manganese over 2% leads to the formation of primary  $\text{Al}_6\text{Mn}$  crystals.

The results of present studies have shown that the phase  $\text{Al}_6(\text{Fe},\text{Mn})$  formed at a manganese content of 1.66 wt.%. The  $\text{Al}_6(\text{Fe},\text{Mn})$  crystals are also enriched with copper. In the alloy investigated the  $\text{Al}_{20}\text{Cu}_2\text{Mn}_3$  phase formation during solidification also reduces the amount of copper and manganese in the solid solution. Due to the refinement and partial dissolution of  $\text{Al}_{20}\text{Cu}_2\text{Mn}_3$  particles upon RSR, the dispersoids precipitation is expected under post-deformation heat treatment.

## 5. Conclusions

The phase composition of Al-1.53Cu-1.66Mn-0.38Zr-0.15Cr-0.15Fe (wt.%) alloy formed during casting has been established. The structure is represented by aluminum solid solution,  $\text{Al}_7\text{Cr}$ ,  $\text{Al}_{20}\text{Cu}_2\text{Mn}_3$  dispersoids and eutectic which

includes  $\text{Al}_6(\text{Fe},\text{Mn})$  and  $\text{Al}_2\text{Cu}$ . Without homogenization of the ingot, RSR at  $280^\circ\text{C}$  results in refining of  $\text{Al}_6(\text{Fe},\text{Mn})$  intermetallics and also in refining and partial dissolution of  $\text{Al}_{20}\text{Cu}_2\text{Mn}_3$  dispersoids, along with microcrystalline structure formation with an average grain size of  $1.6\ \mu\text{m}$ . After deformation, the alloy is characterized by the yield stress of 83 MPa, ultimate strength of 216 MPa and elongation to failure of 25%. The strengthening of the deformed alloy is contributed by an increase in the length of the grain boundaries, solid-solution hardening due to the partial dissolution of dispersoids, and the dispersion of the phases. The supposed deformation induced dissolution of the aluminides gives the potential for further heat treatment of the alloy with the dissolution of the solid solution by manganese, copper and zirconium. Thus, an increase in strength and improvement of the thermal resistance of the alloy are expected.

*Acknowledgments.* The research was supported by Russian science foundation (project No. 22-23-00904). The electron microscopic studies were performed using the equipment of the Collaborative Access Center "Testing Center of Nanotechnology and Advanced Materials" of the IMP UB RAS (Ekaterinburg, Russia).

## References

1. Y. Estrin, A. Vinogradov. Acta Materialia. 61, 782 (2013). [Crossref](#)

2. R.Z. Valiev, R.K. Islamgaliev, I.V. Alexandrov. Prog. Mat. Sci. 45 (2), 103 (2000). [Crossref](#)
3. T.G. Langdon. International Journal of Material Research. 98 (4), 251 (2007). [Crossref](#)
4. R.Z. Valiev, N.A. Enikeev, M.Y. Murashkin, V.U. Kazykhanov, X. Sauvage. Scr. Mater. 63, 949 (2010). [Crossref](#)
5. X. Sauvage, G. Wilde, S. V. Divinski, Z. Horita, R.Z. Valiev. Mater. Sci. Eng. A. 540, 1 (2012). [Crossref](#)
6. Y. Nasedkina, X. Sauvage, E. V. Bobruk, M. Y. Murashkin, R.Z. Valiev, N.A. Enikeev. Alloys Compd. 710, 736 (2017). [Crossref](#)
7. B.B. Straumal, X. Sauvage, B. Baretzky, A. A. Mazilkin, R.Z. Valiev. Scr. Mater. 70, 59 (2014). [Crossref](#)
8. T. Masuda, X. Sauvage, S. Hirosawa, Z. Horita. Mater. Sci. Eng. A. 793, 139668 (2020). [Crossref](#)
9. X. Sauvage, N. Enikeev, R. Valiev, Y. Nasedkina, M. Murashkin. Acta Mater. 72, 125 (2014). [Crossref](#)
10. N. A. Belov, A. N. Alabin, I. A. Matveeva. J. Alloys Compd. 583, 206 (2014). [Crossref](#)
11. N. A. Belov, A. N. Alabin. Mater. Sci. Forum. 765, 13 (2013). [Crossref](#)
12. N. A. Belov, N. O. Korotkova, T. K. Akopyan, K. A. Tsydenov. Metals. 9, 1246 (2019). [Crossref](#)
13. I. J. Polmear. Light Metals: From Traditional Alloys to Nanocrystals, fourth ed. Oxford, Elsevier (2006) 421 p.
14. J. O. Andersson, T. Helander, L. Höglund, P. F. Shi, B. Sundman. Thermo-Calc and DICTRA, Computational tools for materials science. Vol. 26. Calphad (2002) pp. 273–312.
15. G. H. Gulliver. J. Inst. Met. 9, 120 (1913).
16. E. Scheil. Z. Metallkd. 34, 70 (1942).
17. L. F. Mondolfo, Aluminum Alloys: Structure and Properties. London, Butterworths (1976) 806 p. [Crossref](#)
18. N. A. Belov, T. K. Akopyan, P. K. Shurkin, N. O. Korotkova. Journal of Alloys and Compounds. 864, 158823 (2021). [Crossref](#)
19. S. Mondol, S. Kumar, K. Chattopadhyay. Mater. Sci. Eng. A. 759, 583 (2019). [Crossref](#)
20. S. Mondol, S. Kashyap, S. Kumar, K. Chattopadhyay. Mater. Sci. Eng. A. 732, 157 (2018). [Crossref](#)